Supplemental Material

Supplementary material and figures

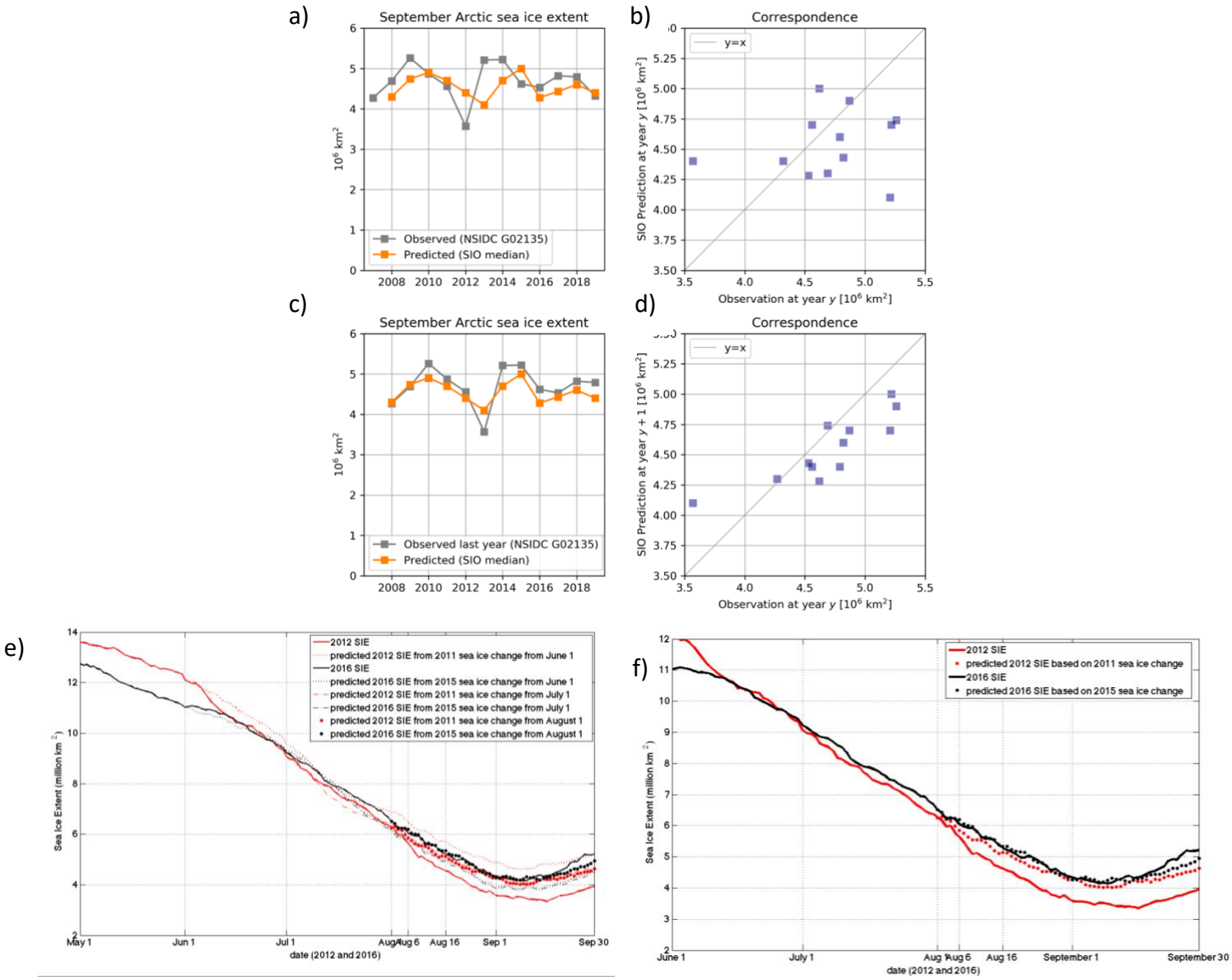

Figure S1. Observed and predicted September Arctic sea ice extent. Weak correspondence between observed and predicted extent shows poor forecast skill (Figures a and b). Correspondence between predicted SIE and previous year's observations shows influence of past year's observations on (statistical and heuristic) forecasts (Figures c and d). Predictions for 2012 and 2016 SIE from e) June, July, and August 1st based on the 2011 and 2015 rates of sea ice loss, respectively, and f) August 1st, following Meier (Sea Ice Outlook, 2016 – 2019), as a specific example of SIO forecasts shown in Figure 1. June, July, and August forecast based on 2011 sea ice loss consistently overestimate 2012 SIE. By contrast the June and July forecast based on 2015 sea ice loss underestimates observed 2016 SIE, while the August forecast approximates (briefly overestimates) 2016 SIE to mid-September and underestimates SIE following.

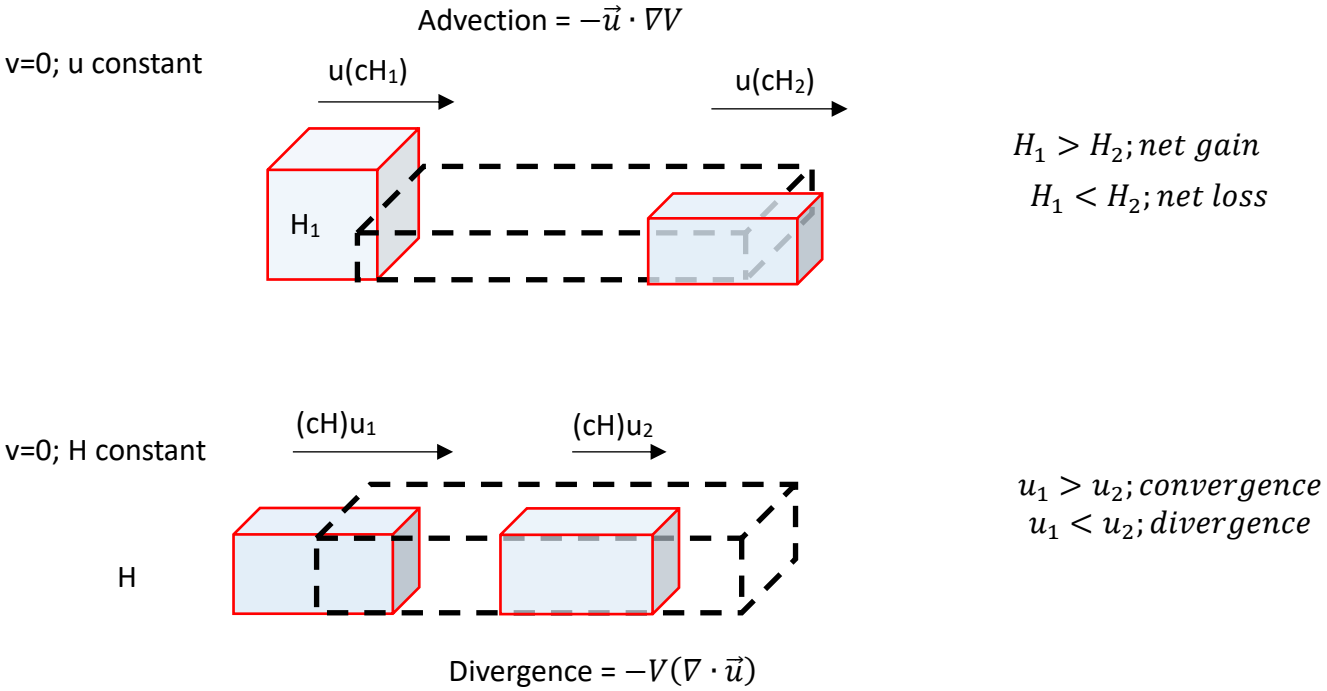

Figure S2. Schematic of sea ice advection (defined here as $-\vec{u} \cdot (\nabla V)$) and divergence (defined here as $-V(\nabla \cdot \vec{u})$) terms (upper and lower panels). For the advection term, ice parcels traveling at the same speed with higher (lower) effective thickness entering than leaving a grid cell results in net sea ice gain (loss). For the divergence term, sea ice parcels with the same effective thickness and higher (lower) speeds entering than leaving a grid cell result in convergence (divergence). In this study, advection > 0 implies that thicker ice moves into the region in the direction of motion, while advection < 0 implies that thinner ice moves into the region in the direction of motion; divergence > 0 (sea ice convergence) implies sea ice accumulation and ridging in a region, while divergence < 0 (sea ice divergence) implies opening of leads and polynyas in the sea ice cover.

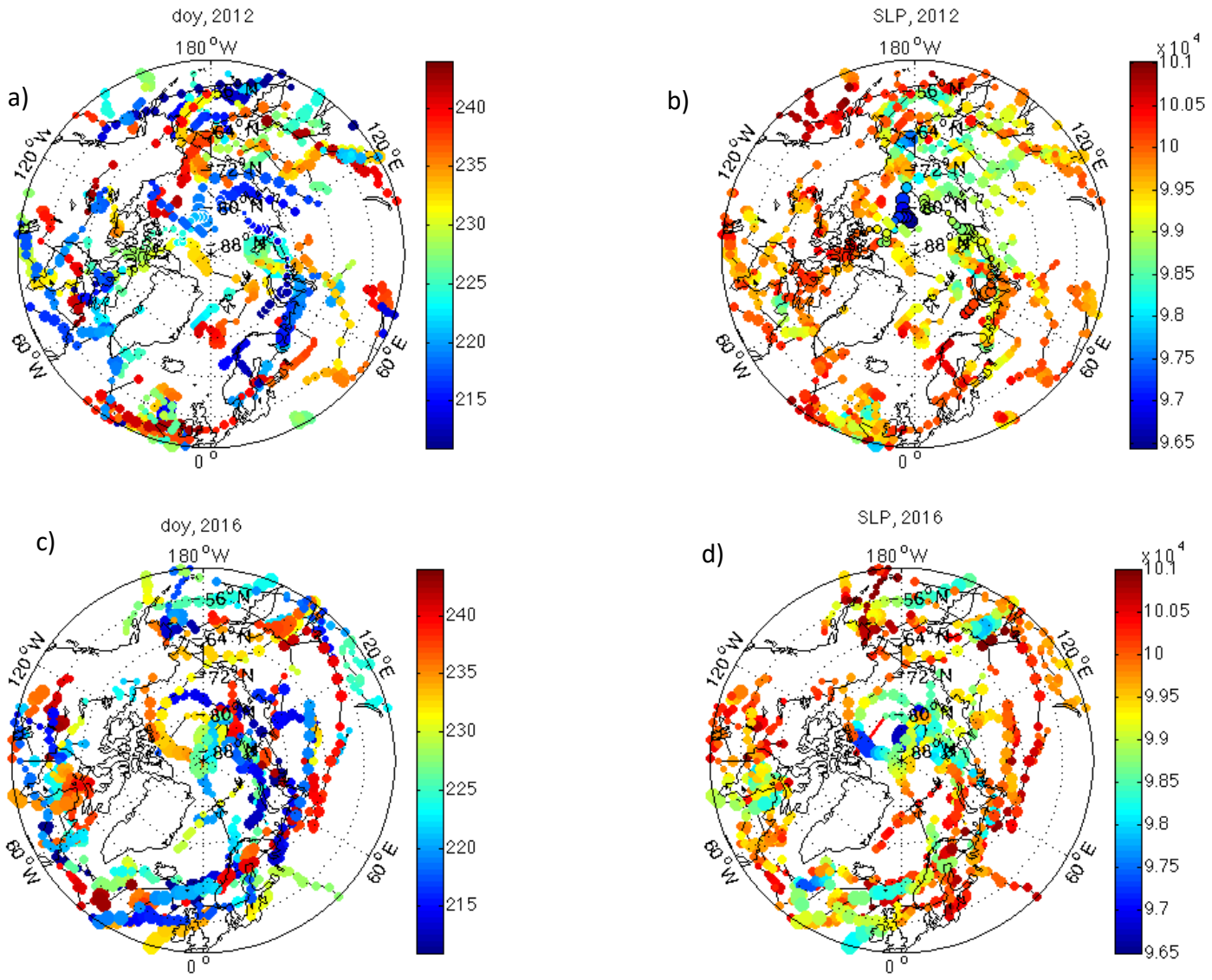

Figure S3. Cyclone trajectories from August 1st to 30th where colours depict a) day of year and b) SLP in 2012 and c) day of year and d) SLP in 2016.

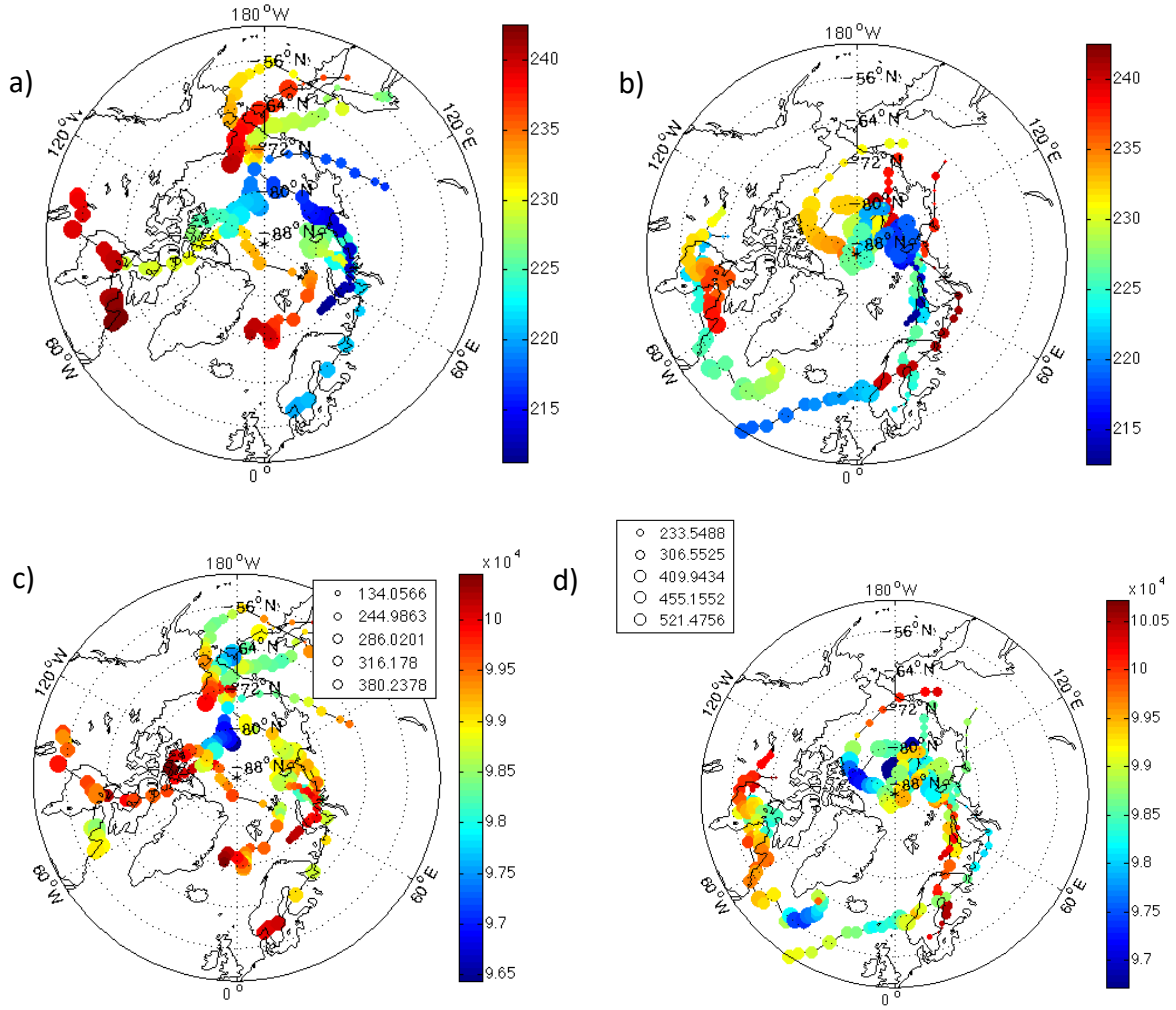

Figure S4. Cyclone trajectories associated with all extreme storms with SLP < 985 hPa in August depicted by day of year in a) 2012, and b) 2016, and SLP in c) 2012, and d) 2016.

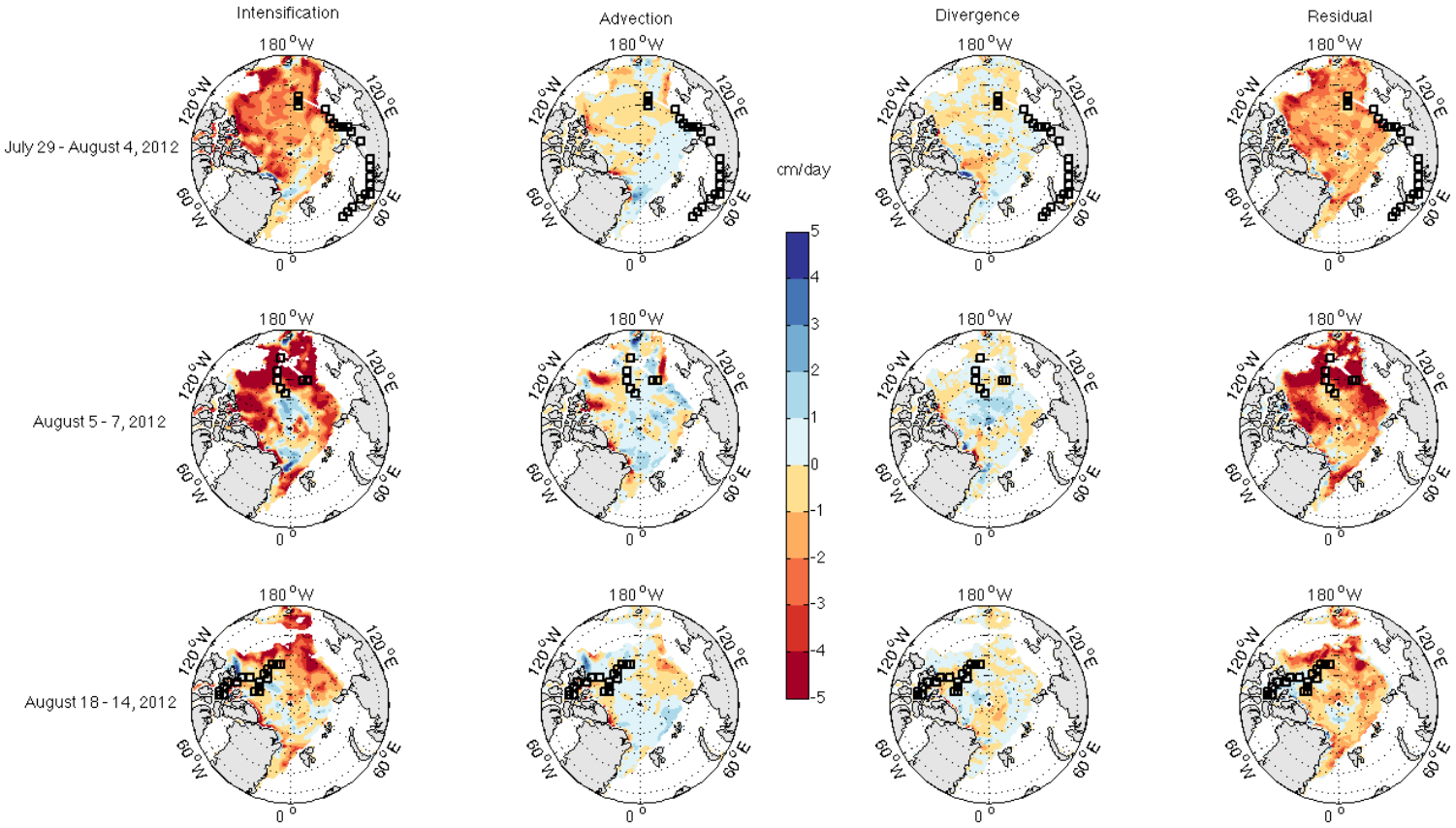

Figure S5. Adjusted sea ice volume budget components including intensification, advection, divergence and residual terms (from left, first, second, third and fourth columns respectively) prior to, during, and following (upper, middle, and lower rows, respectively) the 6 August, 2012 extreme storm using the PIOMAS and NSIDC drift fields combined. Units are in cm/day. Blue (red) indicates sea ice volume increase (decrease).

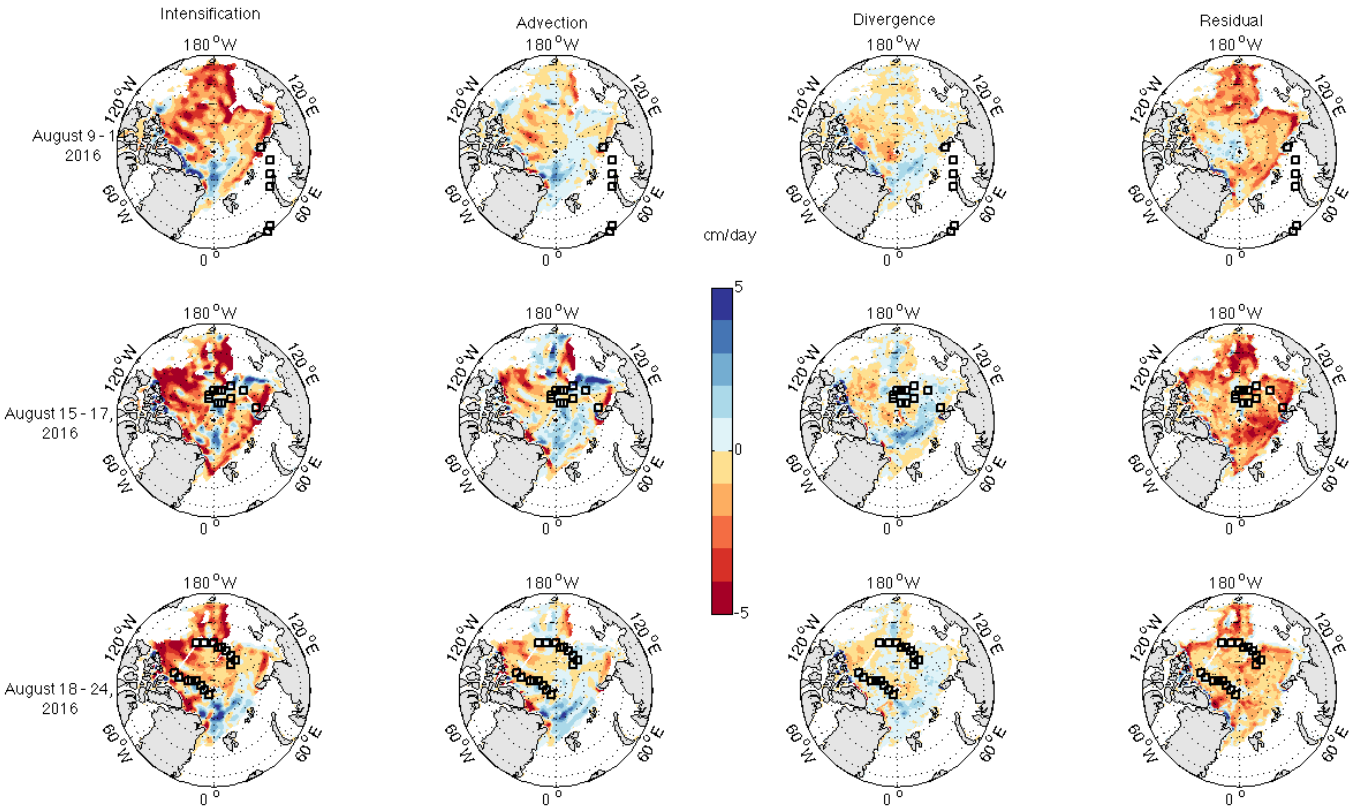

Figure S6. Adjusted sea ice volume budget components including intensification, advection, divergence and residual terms (from left, first, second, third and fourth columns respectively) prior to, during, and following (upper, middle, and lower rows, respectively) the 16 August, 2016 extreme storm using the PIOMAS and NSIDC drift fields combined. Units are in cm/day.

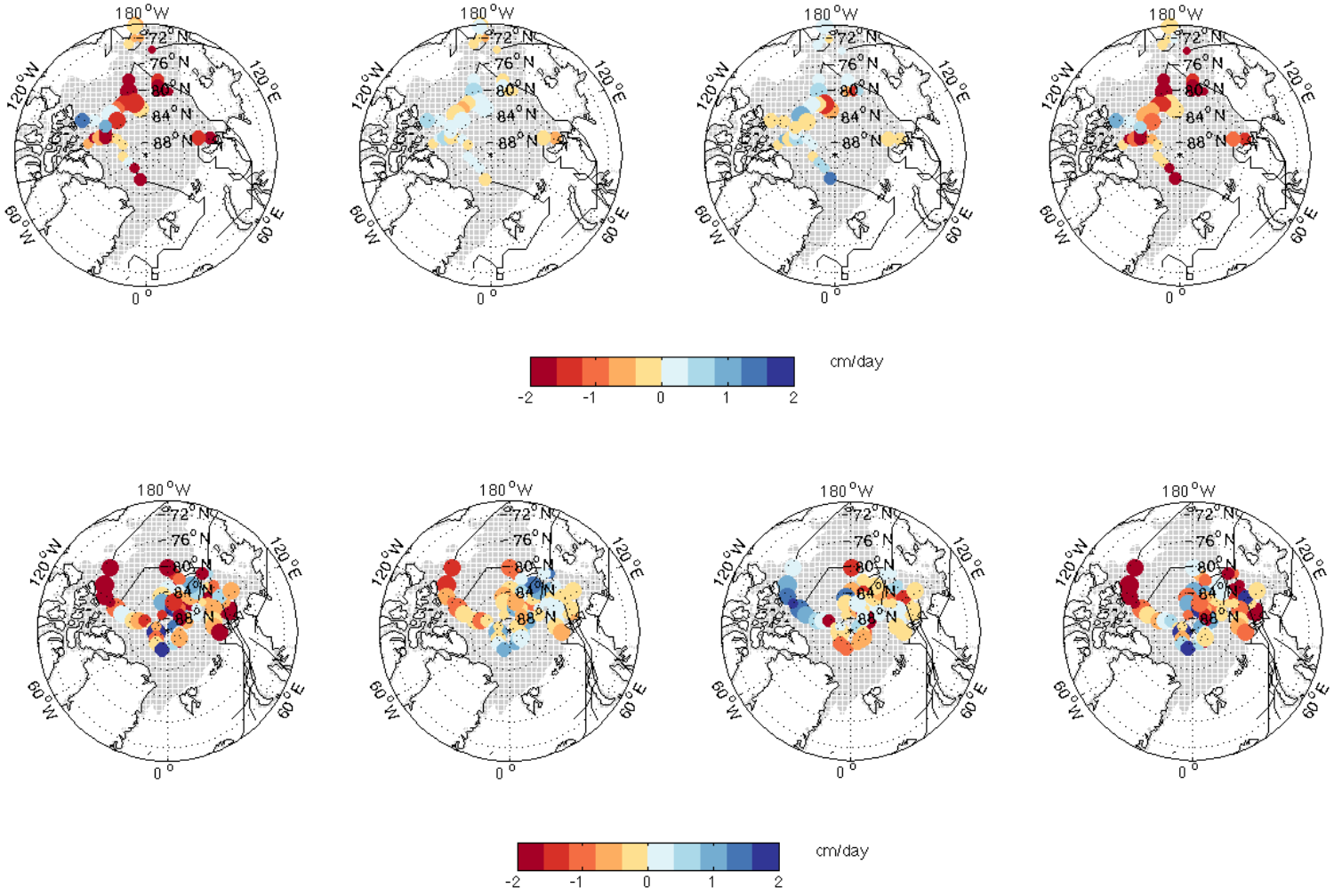

Figure S7. Sea ice volume budget components in the vicinity of storms associated with extreme storm trajectories for 2012 (top row), and 2016 (lower row) showing, from left, the volume intensification, advection, divergence and thermodynamic terms. Units are in cm/day. The shaded area depicts sea ice extent on August 1st.

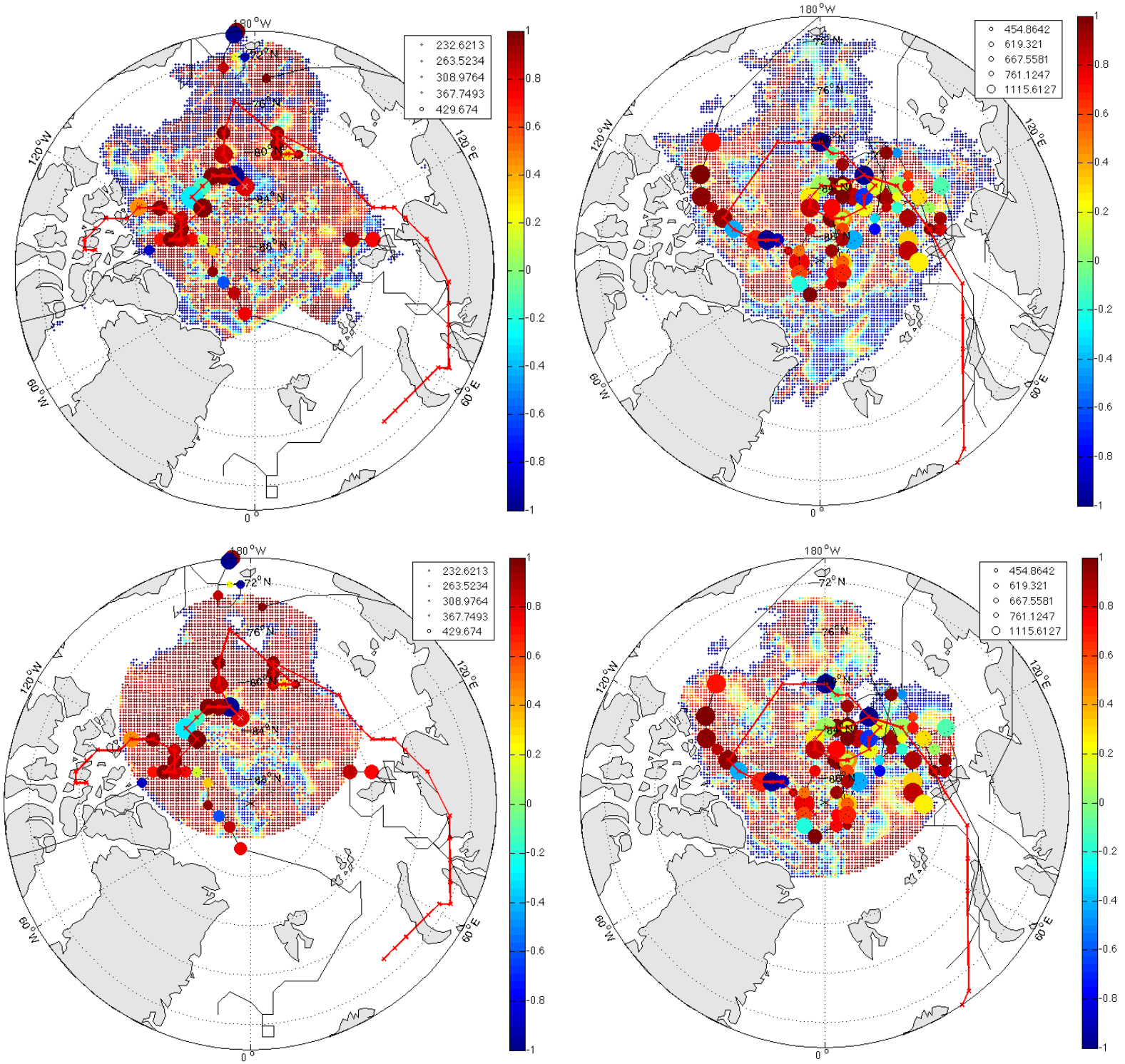

Figure S8. Thermodynamic/dynamic index Q_{td} for storms along and surrounding extreme storm trajectories for 2012 (left) and 2016 (right) with no filter applied. Symbol size depicts variations in storm radius. The upper panels show the superposition of Q_{td} surrounding/within the radius of influence for all cyclones along the extreme storm trajectory. The lower panels show Q_{td} surrounding/within the radius of influence for only the extreme cyclone event associated with the SLP minimum. Red (blue) indicates thermodynamic (dynamic) contributions to changes in sea ice volume.

Sensitivity to spatial scale

We assess the sensitivity of the sea ice volume budget and index Q_{td} index to spatial filtering for a 0, 1, 2, 3 (0, 3x3 (75x75km), 5x5 (125x125 km), and 7x7 (175x175 km) pixel square-window filter applied to sea ice drift field to account for noisy data and artifacts in the NSIDC sea ice drift product (**Figure S9**). Predominantly thermodynamic contributions are observed irrespective of filter near the sea ice edge in 2012. In 2016 dynamic contributions to changes in sea ice volume encompass a larger radius of influence than in 2012; dynamic contributions predominate in the central Arctic with increasing square-window spatial filtering applied, in contrast to 2012, where dynamic/thermodynamic contributions are more sensitive to spatial filtering and spatial scales considered. This once again highlights the non-local impact of storms with large spatial extent on changes in sea ice volume, with implications for coastal communities, shoreline erosion, shipping lanes, renewable energy deployment, and migratory paths of marine mammals.

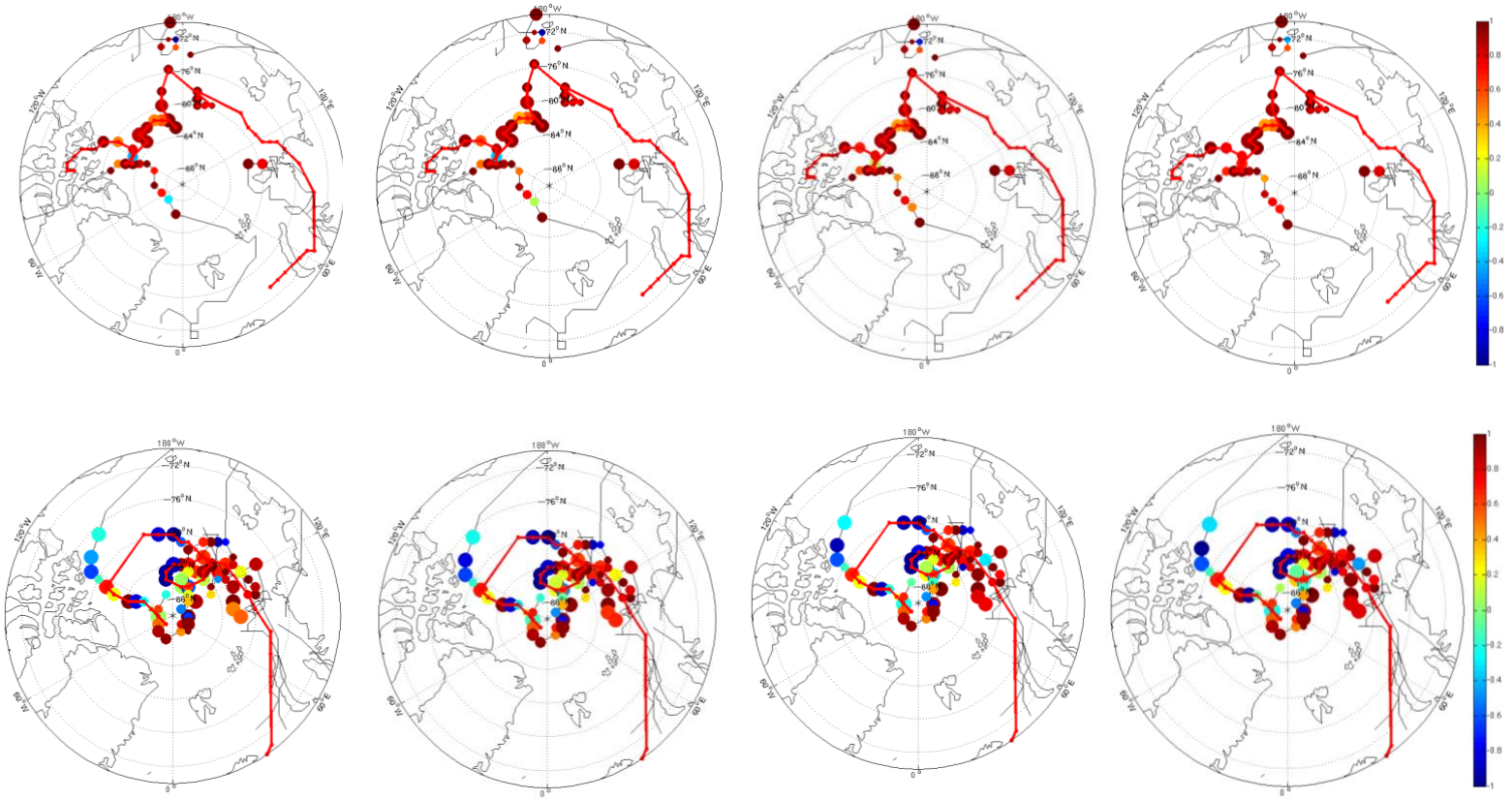

Figure S9. Thermodynamic/dynamic index Q_{td} with, from left, no spatial filtering, 3-pixel, 5-pixel and 7-pixel square-window spatial filtering in 2012 (upper row) and 2016 (lower row).

Standard deviation and uncertainty

Differences in NSIDC and PIOMAS sea ice drift fields and spatial gradients are manifest in the standard deviation in the residual generated using three sea ice drift products (**Figure S10**). Specifically, standard deviation, as a measure of uncertainty, in the residual computed using NSIDC (with and without buoy data) and PIOMAS drift before, during, and following the 2012 and 2016 storms illustrates discrepancy north of Greenland and the Canadian Archipelago, in keeping with past studies showing that maximum discrepancy between PIOMAS and observed sea ice drift occurs in these regions (Zhang et al., 2003), with the exception of the residual/thermodynamic term showing large discrepancy in the central Arctic (Pacific) during (following) the August, 2012 storm and in the central Arctic following the August, 2016 storm (**Figure S10**). The current version of PIOMAS assimilates sea ice concentrations and SSTs, yet not drift (Schweiger et al., 2011), which would account for differences between the modeled and observed ice drift speeds evident in the large standard deviations and uncertainty during the 2012 and 2016 storms.

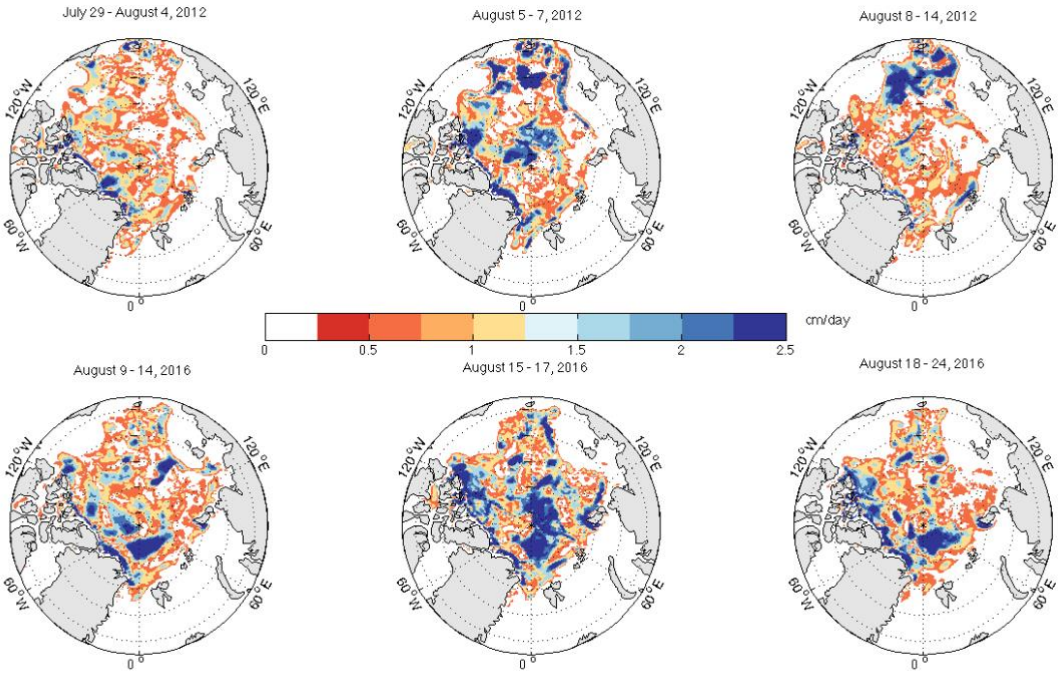

Figure S10. Standard deviation in residual for all three (NSIDC without buoy, PIOMAS, NSIDC with buoy) drift products before, during and following 2012 (upper row) and 2016 (lower row) storm. Units are in m.

The residual term and melt rates

In order to verify whether the residual term provides a realistic estimate of melt rates and thus thermodynamic contributions, we first analyse CICE sea ice model melt rates following Tsamados et al. (2015), sea ice volume budget components using CICE effective thickness and drift, as well as LIM3 sea ice model output to both i) compare model (CICE, LIM3) and PIOMAS/NSIDC results (used in the present study) and ii) evaluate consistency in melt rate values. For simplicity we limit our analysis to 2012. Second, to further evaluate whether residual terms from our analysis are realistic and representative of actual melt rates, we compare melt rates obtained in our analysis with observed melt rates near Fram Strait in August, 2012 from IMB measurements as outlined in West et al. (2020).

Simulated melt rates

Investigation of melt rate components (**Figures S11** and **S12**) and sea ice volume budget components/decomposition (**Figure S14**) from the CICE model illustrates basal melt on the order of 2 - 3 cm/day before the August 8, 2012 storm, enhanced top ice melt and basal melt with total melt exceeding 5 cm/day during the storm, and decelerated melt rates following the storm (Figures S11 and S12). Total melt rates and CICE residual budget component spatial distributions and magnitudes are comparable (Figure S12 compared with fourth column in Figure S14).

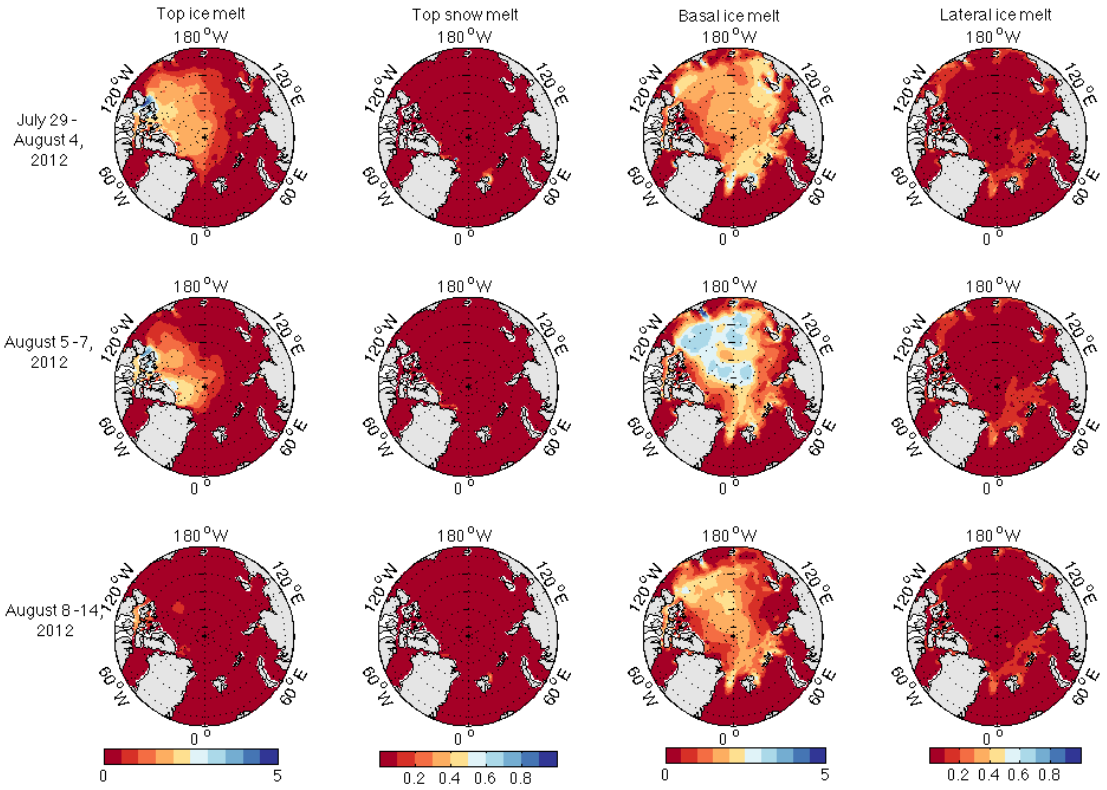

Figure S11. CICE melt rate components (provided by H. Heorton and following Tsamados et al. (2015)) before, during, and following August 2012 extreme cyclone. Units are in cm/day.

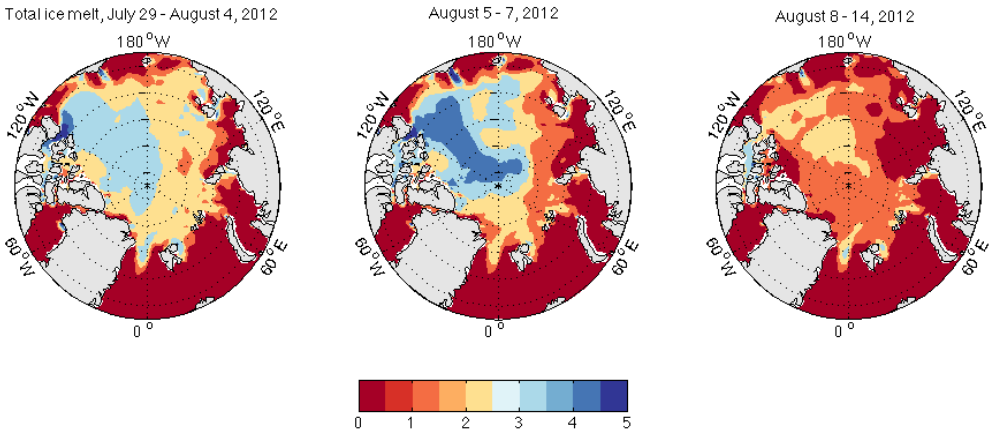

Figure S12. Total CICE melt rates before, during, and following August 2012 extreme cyclone. Units are in cm/day.

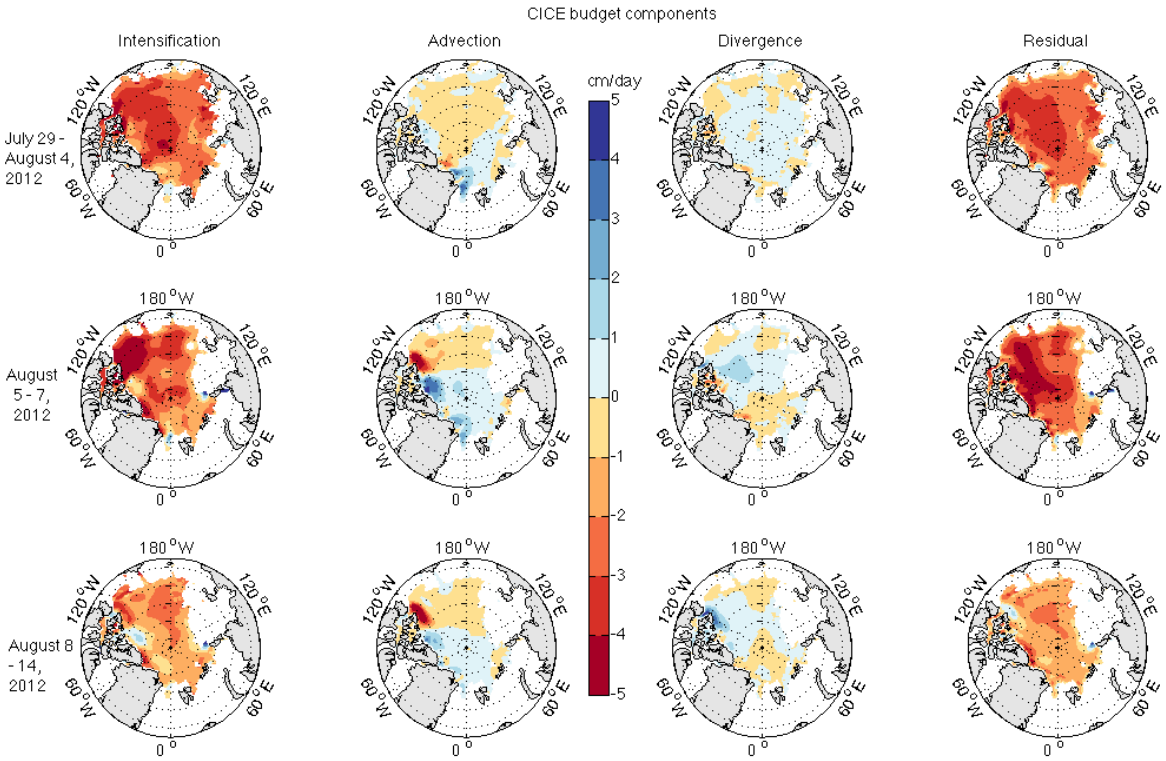

Figure S14. CICE budget components (from left, intensification, advection, divergence, and residual) for 2012 extreme storm using CICE effective thickness and drift. Units are in cm/day.

Furthermore, melt rates from the NEMO-LIM3 global ocean-ice model for the entire month of August in 2012 (following Massonnet et al., 2019, and with monthly output frequency) show mean values ranging from 1 cm/day in the central Arctic to 4 cm/day in the Beaufort Sea region (**Figure S15**). Although the spatial distributions in the simulated (CICE and LIM3) results differ, the magnitudes of the simulated melt rates are comparable to those from the PIOMAS/NSIDC analysis (Figure 7).

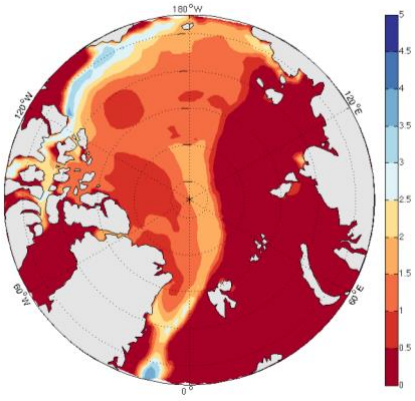

Figure S15. NEMO-LIM3 mean sea ice melt rates for the month of August in 2012. Units are in cm/day.

Observed melt rates

Evaluation of available IMB observations from recent surface flux studies (West et al., 2020) further demonstrates that the residual component provides a reasonable estimate of melt rates (**Figures S16 and S17**). Specifically, changes in ice thickness along IMB trajectories near Fram Strait in 2012 are on the order of 2 cm/day, 6 cm/day, and 1 cm/day before, during, and following, respectively, the August 2012 extreme storm, in keeping with the magnitude of residual component terms. Changes in ice thickness north of Greenland show ice growth rates on the order of 1 – 2 cm/day prior to and during the storm in August, and melt rates on the order of 2 cm/day following, with intervals of ice accumulation, the values of which are also in keeping with the residual term (Figure 7). It should be noted that spatial differences in observed melt rates and those derived from the residual term may be attributed to interpolation and coarse product resolution relative to observations; comparable magnitudes however indicate that the residual term determined from the ice volume budget analysis provides a reasonable estimate of melt rates and thus thermodynamic processes.

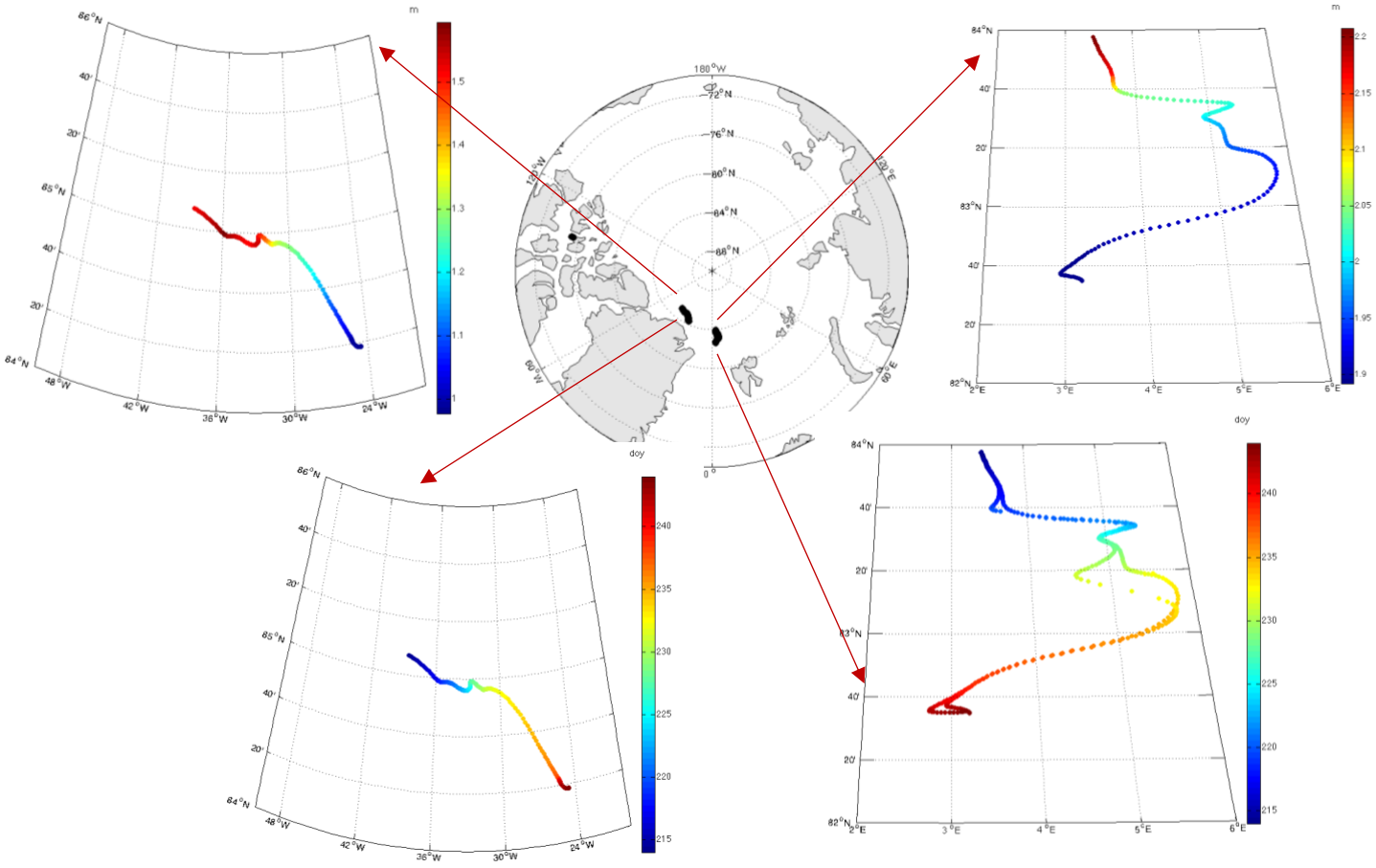

Figure S16. Observed sea ice thickness from IMB measurements during August 2012 as described in West et al. (2020). Lower left (right) panels indicate day of year in 2012, while upper left (right) panels indicate sea ice thickness (in m) associated with IMB measurements north of Greenland (in Fram Strait). Note the difference in scales for thickness measurements. The August 2012 storm occurred on doy 219.

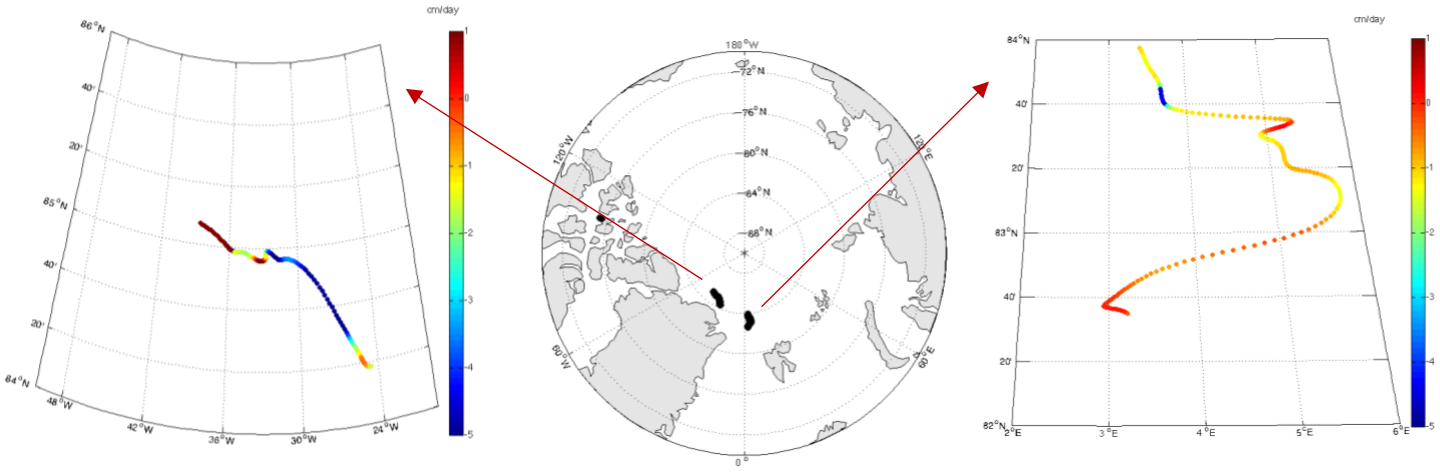

Figure S17. Sea ice melt rates (in cm/day) for IMB trajectories located north of Greenland (left panel) and in Fram Strait (right panel), calculated based on differences in ice thickness along trajectories. In this figure, negative (positive) values indicate sea ice melt (growth).

Comparison of modeled and observed results further reflect the advantage of using observational and even combined observational/reanalysis products over models that do not always capture, and provide differing representations of, physical phenomena.

References

Massonnet, François, Antoine Barthélemy, Koffi Worou, Thierry Fichefet, Martin Vancoppenolle, Clément Rousset, and Eduardo Moreno-Chamarro, 2019: "On the Discretization of the Ice Thickness Distribution in the NEMO3.6-LIM3 Global Ocean–Sea Ice Model." *Geoscientific Model Development* 12, no. 8, 3745–58. https://doi.org/10.5194/gmd-12-3745-2019.

West, A., Collins, M., and Blockley, E.: Using Arctic ice mass balance buoys for evaluation of modelled ice energy fluxes, Geosci. Model Dev., 13, 4845–4868, https://doi.org/10.5194/gmd-13-4845-2020, 2020.

Zhang, J., D. R. Thomas, D. A. Rothrock, R. W. Lindsay, Y. Yu, and R. Kwok, Assimilation of ice motion observations and comparisons with submarine ice thickness data, J. Geophys. Res., 108(C6), 3170, doi:10.1029/2001JC001041, 2003.